A Novel Energy Router Based on Multi-winding Line Frequency Transformer

Zhitao Guan[1], Dan Wang[1], Qing Duan[2], Chengxiong Mao[1*], Bin Liu[1]

[1] School of Electrical and Electronic Engineering, Huazhong University of Science and Technology, Wuhan, China
[2] Beijing Key Laboratory of Distribution Transformer Energy-saving Technology, China Electric Power Research Institute, Beijing, China
[*] cxmao@hust.edu.cn

Abstract: Energy routers based on the electronic power transformer are suitable for the AC-DC hybrid grid with multiple voltage levels, but their structures are complex. This paper proposes a novel energy router based on the multi-winding line frequency transformer. By a combination of a multi-winding line frequency transformer and power electronic devices, the proposed energy router can take advantage of the high reliability of the multi-winding line frequency transformer and the high controllability of power electronic devices. The proposed energy router is suitable for the AC-DC hybrid grid with multiple voltage levels and has the characteristic of a simple structure. The simulations and experimental results demonstrate the effectiveness of the proposed energy router.

1. Introduction

Recently, the environmental pollution, and energy shortage caused by fossil fuels have attracted widespread attention in various countries [1], and there are large amounts of renewable energy resources connected to grids. The rapidly increasing renewable energy integration increases the need for smarter energy management [2]. The concept of energy routers (ERs) is proposed to provide plug-and-play interfaces for distributed renewable energy resources, energy storage devices, and loads [3]. ER can also improve the controllability of the smart grid [4], [5], including active controls of bidirectional flows of energy, power quality control, and energy management optimization [3], [6]-[11].

Generally, ER is based on multi-port converters (ER-MPC) [3], [12]-[15] or the electronic power transformer (ER-EPT) [16]-[18]. ER-MPC is beneficial to the access of various forms of renewable energy resources [12]-[15], the unified design of the interface [15], and the coordinated control of multiple converters [12]-[14]. ER-MPC is not suitable for the grid with multiple voltage levels, as it cannot provide galvanic separation between ports. ER-EPT can meet the need of high-voltage and large-capacity scenarios and can provide DC ports with multiple voltage levels [16]. ER-EPT can achieve galvanic separation between ports by medium-frequency transformers [17], [18], and is suitable for the AC-DC hybrid grid with multiple voltage levels. The structure of ER-EPT is complex due to its multi-level converters, which leads to complex control [16], [19].

Line frequency transformers (LFTs) are widely used in power systems, which can provide voltage scaling and galvanic separation [16], and have the characteristics of a simple structure. The concept of a hybrid distribution transformer (HDT) is proposed by the combination of LFTs and power electronic devices [20], [21]. HDT can take advantage of the high efficiency and reliability of LFTs and the high controllability of power electronic devices [19], and also meet the demand of the smart grid [22]-[24].

A novel energy router based on multi-winding LFT (ER-MLFT) is proposed in this paper. ER-MLFT couples energy by MLFT, which can also achieve galvanic separation between each port. ER-MLFT can take advantage of the high reliability of MLFT and the high controllability of power electronic devices. ER-MLFT is suitable for the AC-DC hybrid grid with multiple voltage levels and has the characteristic of a simple structure. Essentially, ER-MLFT is a combination of ER-MPC and HDT.

Section 2 presents the structure and characteristics of ER-MLFT. Section 3 describes the control strategy, including the upper-level control and the lower-level control. In Sections 4 and 5, the simulation and experimental results are provided to verify the effectiveness of the control strategy and the practicality of ER-MLFT.

2. Concept of ER-MLFT

ER provides plug-and-play interfaces for devices of different voltage types and levels, and realizes electrical isolation between interfaces. Another important function is local power management functions, such as energy management, suppressing fluctuations of port voltages, power quality management, and increasing power supply reliability [6]-[11].

2.1 ER-MLFT Structure

Fig. 1 (a) describes the system constructed by the ER-MLFT, which is called the energy subnet [12]. Port 1 is for the medium-voltage (MV) power grid. Port 2 can transmit power to AC loads and provide access to the microgrid. Port 3 is used to connect distributed energy resources (e.g., photovoltaic, wind power, and fuel cell), distributed DC energy storage devices (e.g., chemical battery), and DC loads (e.g., electrical vehicle, and rail). Port 4 provides a low-voltage (LV) DC bus and transmits power to DC loads (e.g., residential/office buildings). Port 5 is for a doubly-fed induction generator (DFIG)-based on wind farms.

Fig. 1 (b) shows the main circuit topology of ER-MLFT, and ER-MLFT constants of six parts: MLFT T_1, Converter A, Converter B, Converter C, Converter D, and the

series transformer T_2. The MLFT T_1 is the core component of ER-MLFT and couples the energy from different ports.

Winding w_{11} provides an interface for the MV power grid. Winding w_{12} supplies an AC port for DFIG-based on wind farms by design. Winding w_{13}, and w_{14} are for Converter D and Converter C, respectively. To improve the controllability and flexibility of ER-MLFT, converter A and Converter B are employed. The current harmonic compensation, reactive power compensation, and asymmetry compensation for non-linear load from Port 2 are achieved by Converter B. Converter A and T_2 work together for the fluctuation and harmonic compensation of grid voltage. Furthermore, when ER-MLFT transmits power to the distribution grid, line loss may become significant with heavy power injection [11], and Converter A can compensate for the line loss through the series transformer T_2.

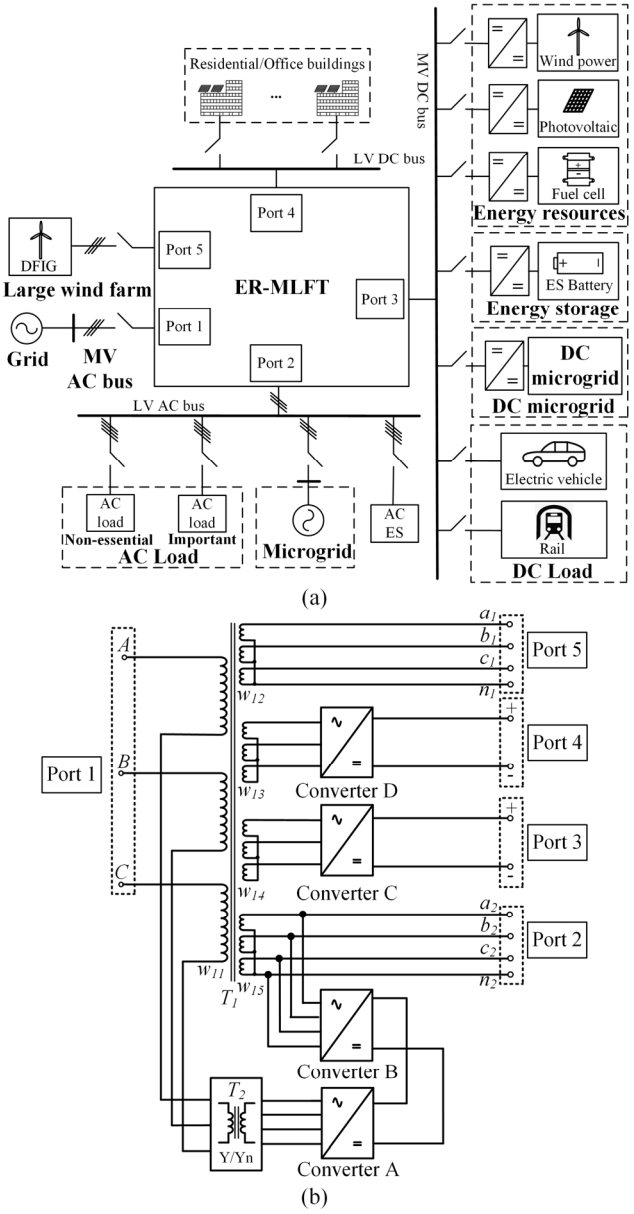

Fig. 1. *The structure of ER-MLFT. (a) Energy subnet. (b) Main circuit topology.*

2.2. The Characteristics

By a combination of a MLFT and power electronic devices, ER-MLFT can take advantage of the high reliability of the MLFT and the high controllability of power electronic devices. The following characteristics are attractive:

1) **Energy routing.**

ER-MLFT couples energy from ports by MLFT and converters, and enables bidirectional flow of energy between ports. Port power information is collected to the upper control. When the power step, ER-MLFT can respond quickly and suppress voltage fluctuations.

2) **Power quality management function.**

Converter B is employed for non-linear load from Port 2. Besides, Converter A can maintain the voltages of MLFT at the rated value and mitigate the harmonics. ER-MLFT can improve the quality of load current and power supply voltage, and meet the functional requirements of ER.

3) **High safety and reliability.**

ER-MLFT provides galvanic separation between each port by MLFT and has the characteristic of a simple structure. Besides, the protection strategies for LFTs are relatively mature, which can be employed in ER-MLFT. Due to the characteristic of a simple structure, the reliability of ER-MLFT is higher than that of ER-EPT.

4) **Multiple voltage level conversion.**

For the sake of brevity, ER-MLFT in Fig. 1 contains five ports. According to the actual need, more AC and DC ports in different voltage levels can be provided by an association of MLFT and rectifiers. For example, the output voltage of DFIG-based on wind farms is usually 690-V, and ER-MLFT provides a 690-V AC port (Port 5) for DFIG-based on wind farms. The 10-kV/690-V power transformer is not required.

3. The control frame of ER-MLFT

As shown in Fig. 2, there are two layers of control in the ER-MLFT system: the upper-level and lower-level controls. The upper-level controls include two layers: the management layer and the information layer, and the lower-level controls are for the function of multiple converters and breakers.

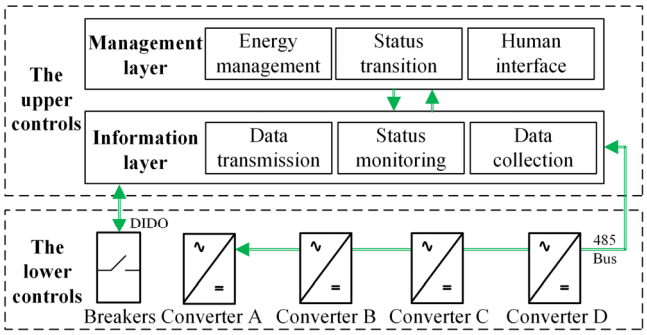

Fig. 2. *The control frame of ER-MLFT.*

3.1. *The Upper-level Controls*

3.1.1 Management layer

1) Energy management.

One of the most important functions of ER-MLFT is coordinated control of distribution grid, microgrid, distributed generation, load, and energy storage. The energy coupling of

the ER-MLFT is based on MLFT. Energy management strategy can be employed based on the coupling form.

When ER-MLFT is in grid-connected mode, Port 1 balances energy of the system, and energy storage (ES) devices work for the high economy, low loss, etc. When ER-MLFT is in islanded mode, ES devices of Port 2 and Port 3 balance the energy of the system.

2) Status transition.

This part is for mode transition and power step. The upper-level controls guarantee the accuracy and stability during mode transition, such as selecting the appropriate mode according to data from the information layer, stabilizing voltage amplitude and frequency from grid tie to islanded mode, etc. The upper-level controls also suppress the voltage fluctuations when power steps. Especially, when power steps in islanded mode, ER-MLFT needs to balance the power of each port.

To achieve good transition performance, Converter C and the DC ES work together to stabilize the voltage and balance power of each port. The feedforward compensation $i^*_{3d\_Feed}$, $i^*_{3q\_Feed}$, and $i^*_{ES_}$Feed are employed. The grid power in islanded mode is zero. Before the grid is at fault, the value of power is recorded. The values of $i^*_{3d\_Feed}$, $i^*_{3q\_Feed}$, and $i^*_{ES\_Feed}$ are calculated according to the difference of grid power in grid-connected mode and islanded mode.

Assuming the measured voltage and current of MLFT port i are U_{d_i} and $I_{d\_i} + jI_{q\_i}$, the equivalent impedance and the predicted power at rated voltage can be expressed as (1) and (2), respectively.

$$Z_{eq\_i} = \frac{U_{d\_i}}{I_{d\_i} + jI_{q\_i}} \tag{1}$$

$$P_{pr\_i} = \frac{U^2_{rated\_i}}{Z_{eq\_i}} \tag{2}$$

The predicted power change ΔP_i is the difference between the recorded power P_{re_i} and the predicted power P_{pr_i}. The values of $i^*_{3d\_Feed}$, $i^*_{3q\_Feed}$ and $i^*_{ES\_Feed}$ are calculated according to the sum of the predicted power changes except for ΔP_3 ($\Sigma\Delta P_i$ - ΔP_3).

When the grid fault is cleared, ER-MLFT can control the frequency and amplitude of output voltage of Converter C to achieve grid connection.

3) Human interface.

This part is designed for user needs, including the choice of optimization goal of energy path, the setting of important loads, the limitation of charging current of the battery, etc.

3.1.2 Information layer

The high concentration of information is a major feature of ERs. The goal of the information layer is to share data in real-time to achieve optimization of the energy path. The information layer needs to collect data from the lower-level controls and management layer and transmit them between the lower-level controls and management layer. The data consists of voltages, currents, power, frequency, and the command value. Moreover, the information layer provides the function of status monitoring, including the status of devices connected to the ports, the operation mode of ER-MLFT, the coordinated operation mode of multiple ER-MLFT, etc.

3.2. *The Lower-level Controls*

The lower-level controls are provided by converters of ER-MLFT, and regulate voltages of AC and DC buses or provide power/frequency control. Fig. 3 shows the lower-level controls for converters. And the command in Fig. 3 is described in Table 1. Converter D is an LV DC rectifier, and its control is the same as that of Converter C (MV DC rectifier) in grid-connected mode and is not described in detail. Besides, the control of energy storage battery is considered, because it is important for ER-MLFT in islanded mode.

Table 1 The description of ER-MLFT's control command.

	Description
$U^*_{i\_abc}$	expected fundamental positive sequence component value of $U_{i\ abc}$, e.g. 10 kV.
$U^*_{dc\ MV}$	reference of MV dc port voltage $U_{dc\ MV}$, e.g. 750 V.
$U^*_{dc\ LV}$	reference of LV dc port voltage $U_{dc\ LV}$, e.g. 400 V.
i^*_{s3q}	reference of q-axis current of i_{s3q}, related to reactive power.
U^*_{3rms}	reference of Port 3 voltage amplitude in islanded mode.
f^*_3	reference of Port 3 ac voltage frequency in islanded mode.
$i^*_{3d\ Feed}$	d-axis feedforward compensation of Converter C.
$i^*_{3q\ Feed}$	q-axis feedforward compensation of Converter C.
$U^*_{dc\ com}$	reference value of the common dc bus, same as $U^*_{dc\ MV}$.
$i^*_{4i\_abc}$	fundamental positive sequence active component value of $i_{4i\ abc}$.
i^*_{ES}	reference of charging/discharging current of ES battery.

The control goal of Converter A is to smooth the input voltage of the MLFT and mitigate harmonics in the distribution grid. The in-phase compensation method is adopted. The injected voltage is in phase with the source voltage, which means that the $U^*_{i\_abc}$ (Fig. 3 (b)) is in phase with that of E_{s_abc}.

Converter B mainly performs power quality management for the load current of Port 3 (LV AC port). As shown in Fig. 3 (c), the PI controller and the repeat controller are employed in parallel [25]. The $i^*_{4i\_abc}$ is the fundamental positive sequence component of I_{4o_abc}. The predicted voltage of input inductance L can be expressed as (3).

$$U^*_{L\_a} = \frac{i^*_{L\_a} - i^*_{L\_a} \times Z^{-1}}{T_{sample}} \times L \tag{3}$$

where T_{sample} is the sample period, and Z^{-1} is a unit delay.

Converter C is a MV rectifier and Fig. 3 (d) indicates that the double closed-loop controller is employed in Converter C in grid-connected mode. The controller includes the outer loop for DC voltage and the inner loop for grid currents. The control goal is to maintain DC voltage at the rated value while getting sinusoidal input currents. In islanded mode, Converter C works to regulate the voltages of MLFT ports, provided that there is enough reactive and active power (from ES battery) to supply all of the critical loads. The outer loops of reactive and active power stabilize the amplitude and frequency of AC side voltage respectively [26]. Feedforward compensation $i^*_{3d\_Feed}$, $i^*_{3q\_Feed,}$ and $i^*_{ES\_Feed}$ are designed for mode switching and power fluctuation in islanded mode. Instead of Converter C, the ES battery from the MV DC port maintains DC voltage at the rated value.

As shown in Fig. 3 (e), in grid-connected mode, the ES battery works in the desired charging/discharging state. In islanded mode, the ES battery maintains DC voltage at the rated value instead of Converter C.

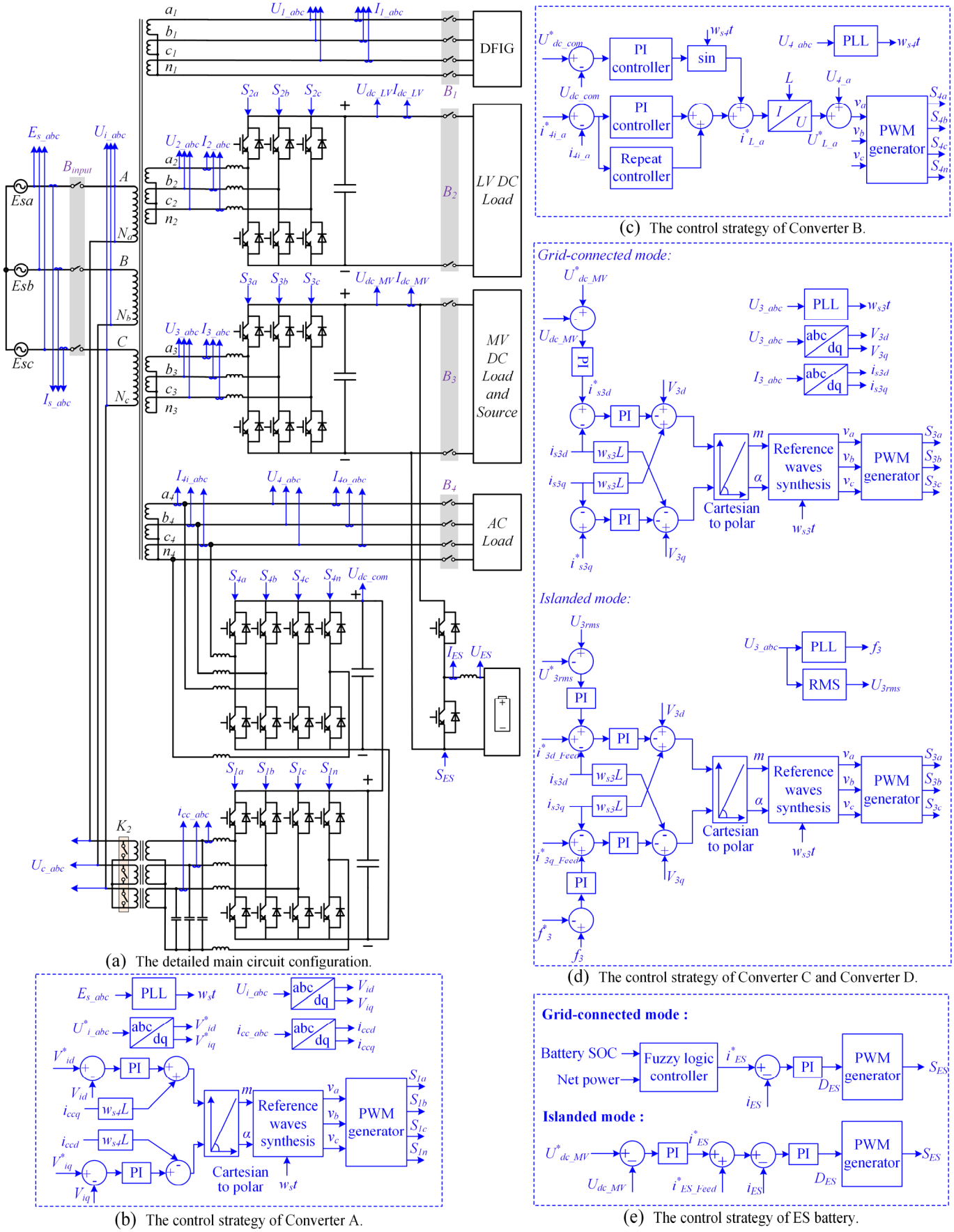

(a) The detailed main circuit configuration.

(b) The control strategy of Converter A.

(c) The control strategy of Converter B.

(d) The control strategy of Converter C and Converter D.

(e) The control strategy of ES battery.

Fig. 3. *The lower control strategy of ER-MLFT. (a) The detailed main circuit configuration. (b) The control strategy of Converter A. (c) The control strategy of Converter B. (d) The control strategy of Converter C and Converter D. (e) The control strategy of ES battery.*

4. Simulation results

The simulation model of the ER-MLFT in Fig. 3 is established in MATLAB/Simulink. The rated power of DFIG, PV, and ES are 50-kVA, 100-kVA, and 70-kVA, respectively. The maximum load power of the MV DC bus, LV DC bus, and 380-V AC bus are 100-kVA, 20-kVA, and 100-kVA, respectively. The rated ratio w_{11}:w_{12}:w_{13}:w_{14}:w_{15} of the MLFT T_1 is 10-kV:690-V:380-V:200-V:380-V, and the rated ratio w_{21}:w_{22} of T_2 is 1-kV:380-V. The MV DC source in the simulation model employs the PV model and ES battery. Maximum power point tracking (MPPT) is used to fully utilize the PV output power. By adjusting the charging current, ES battery controls output power in grid-connected mode and maintains MV DC voltage at the rated value in islanded mode.

4.1. *Case A: Mode Switching Between Grid-Connected Mode and Islanded Mode.*

Assuming the grid voltage is at the rated value and the 380-V AC port is connected with the linear load, Converter A and Converter B do not work. The grid-connected method adopts the first one in section 3. The distribution grid fails at 1 s and recovers at 4 s. The power of AC load decreases from 85 kVA to 65 kVA at 2 s, and the power of PV drops from 100 kVA to 60 kVA at 3 s. The power of DFIG, MV DC load, and LV DC load are 45 kW, 90 kW, and 16 kW, respectively.

As shown in Fig. 4, when ER-MLFT is changed into islanded mode at 1 s or AC load power steps at 2 s, it takes about two fundamental cycles (40 ms) to stabilize the voltage and there is a slight distortion of the AC voltage of ER-MLFT. When PV output power changes at 3 s, ES battery balances the active power and the fluctuation range of MV DC voltage is controlled within ±5 V. ER-MLFT connects to the grid at 4.012 s, and it takes 0.012 s to finish the grid connection process.

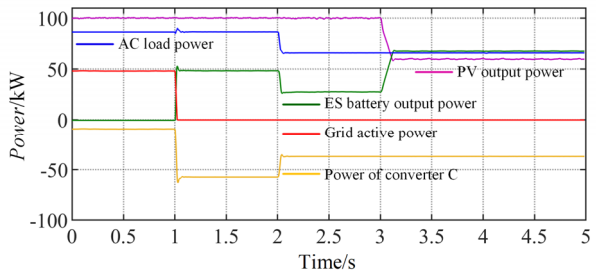

Fig. 4. *The simulation waveforms of ER-MLFT in Case A.*

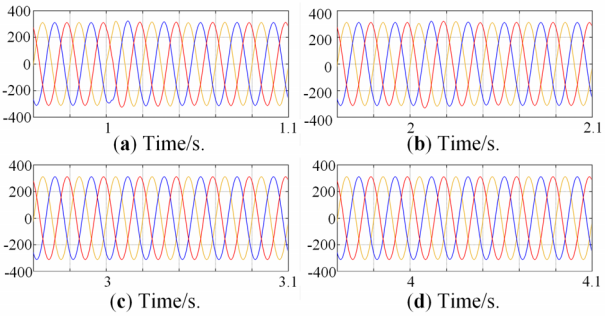

Fig. 5. *The detailed waveforms of U_{1_abc} in Case A.*

The detailed waveforms of U_{1_abc} is shown in Fig. 5. The waveform of U_{1_abc} only fluctuates slightly at 1 s. The simulation results indicate the good transient performance of ER-MLFT (even in islanded mode) and the effectiveness of transient control for ER-MLFT.

4.2. *Case B: The Power Quality Management.*

This case is designed to verify the effectiveness of Converter A and Converter B in the function of power quality management. In this case, the grid voltage is composed of the fundamental wave (The RMS of line voltage is 9.5 kV) and the fifth harmonic (The RMS of 250 Hz line voltage is 500 V). A parallel association of highly inductive nonlinear loads (composed of a series connection of a diode bridge, a 14 Ω resistance and 10 mH inductance), and a three-phase asymmetric RCL series load (phase a: 7 kW and 3 kVar, phase b: 4.5 kW and 6 kVar, phase c: 4.5 kW and 3 kVar.) are connected to 380-V AC port.

Fig. 6 and Table 2 indicate the simulation waveforms and simulation calculated results of voltages and currents. The results verify the effectiveness of power quality management function. The reason why the fundamental RMS of I_{4i_abc} is over I_{4o_abc} is that the operation of Converter A requires power. The simulation results indicate that Converter A can support the fundamental voltage and mitigate the voltage harmonics, and Converter B can compensate for harmonic, reactive power, and asymmetry.

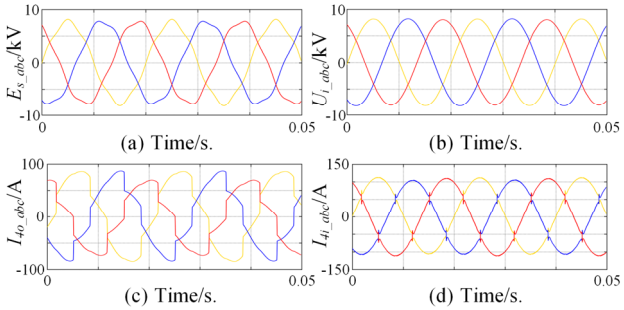

Fig. 6. *The simulation waveforms of ER-MLFT in Case B. (a) The grid voltage. (b) The voltage of 10-kV port. (c) The load current. (d) The MLFT's output current.*

Table 2 The simulation calculated results in Case B.

Parameter	Value
THD of $E_{s\ abc}$	5.26%, 5.26%, 5.26%
THD of $U_{i\ abc}$	0.28%, 0.27%, 0.30%
Fundamental RMS of $E_{s\ abc}$	5.484 kV, 5.484 kV, 5.484 kV
Fundamental RMS of $U_{i\ abc}$	5.787 kV, 5.812 kV, 5.698 kV
THD of $I_{4i\ abc}$	2.95%, 3.05%, 2.94%
THD of $I_{4o\ abc}$	14.06%, 15.32%, 17.37%
Fundamental RMS of $I_{4i\ abc}$	77.5 A, 75.2 A, 78.3 A
Fundamental RMS of $I_{4o\ abc}$	61.7 A, 56.4 A, 50.3 A
The reactive power provided by $I_{4i\ abc}$	0.38 kVar
The reactive power provided by $I_{4o\ abc}$	12.02 kVar

5. Experimental Results

A 100-kVA experimental prototype is developed. Converter D in Fig. 1 is a conventional LV rectifier, and is not included in the experimental prototype. The prototype and its topology are shown in Fig. 7.

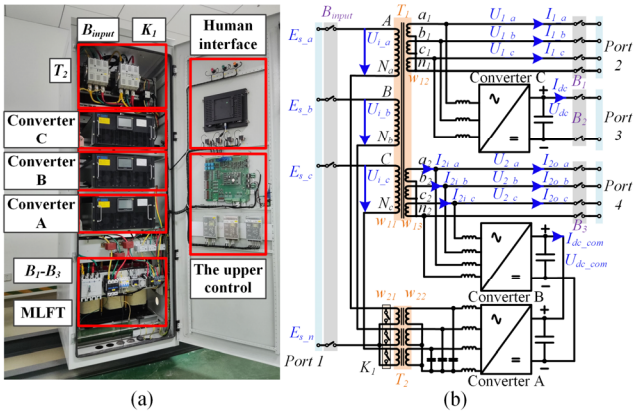

(a) (b)

Fig. 7. *The experimental prototype of ER-MLFT. (a) The experimental prototype. (b) The topology of the prototype.*

The rated voltages of Port 1, Port 2, Port 3, and Port 4 are 380-V (AC), 380-V (AC), 750-V (DC), and 380-V (AC), respectively. Their rated capacities are 100-kVA, 60-kVA, 20-kVA, and 20-kVA, respectively. The rated ratio w_{11}:w_{12}:w_{13} and capacity of T_1 are 380-V:380-V:380-V and 100-kVA. The rated ratio w_{21}:w_{22} and capacity of T_2 are 24-V:207-V and 12-kVA. The phase voltage reference of U_{i_abc} is 220(±3)-V.

5.1. CASE A: Steady-state of ER-MLFT.

Since the maximum compensation degree of Converter A is 10%, the rated load of the prototype is 90 kVA. When the phase voltage of the grid is 240.5 V, the steady-state experimental waveforms with 90-kVA load are shown in Fig. 8.

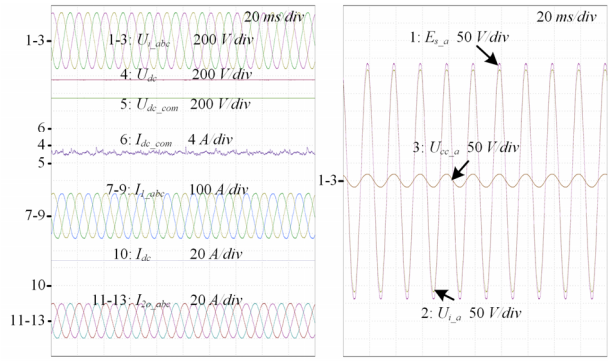

(a) (b)

Fig. 8. *The steady-state waveforms in with the 90-kVA load. (a) The steady-state waveforms. (b) The voltages of Port 1.*

Fig. 8(a) indicates that the voltages and currents of ports are maintained at each rated value. The results in Fig. 8(b) show that the peak voltages of E_{s_a}, U_{i_a}, and U_{cc_a} are 337 V, 316 V, and 20 V. The RMS of U_{i_a} is 223.4 V, while its phase voltage reference is 220(±3) V. Thus the dynamic voltage regulation function of ER-MLFT is verified.

5.2. Case B: Step of Load Power.

The responses of ER-MLFT to several different events are shown in Fig. 9. These events are also summarized in Table 3. The results shown in Fig. 9 indicate that U_{i_abc} and U_{dc} have a minor fluctuation and restore to stability state quickly when switching on the 90-kVA rated load, and thus verify the good transition performance of the proposed ER-MLFT.

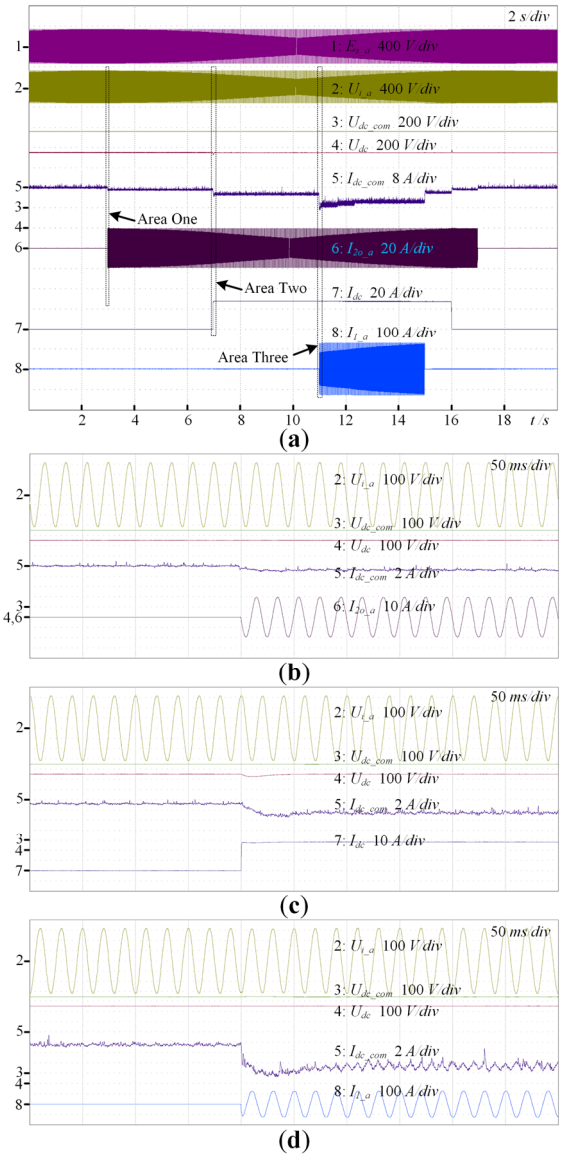

Fig. 9. *The ER-MLFT experiment waveforms in Case B. (a) The voltages and currents. (b) The detailed waveforms of Area One. (c) The detailed waveforms of Area Two. (d) The detailed waveforms of Area Three.*

Table 3 The experimental events in Case B.

Time	Event
3s	The load power of Port 4 is increased from 0 to 10 kVA.
7 s	The load power of Port 3 is increased from 0 to 20 kVA.
11 s	The load power of Port 2 is increased from 0 to 60 kVA.
15 s	The load power of Port 2 is decreased from 60 kVA to 0.
16 s	The load power of Port 3 is decreased from 20 kVA to 0.
17 s	The load power of Port 4 is decreased from 10 kVA to 0.

5.3. Case C: The Power Quality Management.

ER-MLFT provides not only power supplies of different voltage levels and different voltage types, but also power quality management, such as harmonic compensation, reactive

power compensation, asymmetry compensation, etc.

To verify the power quality management function, the responses of ER-MLFT to several different cases are shown in Fig. 10. Table 4 summarizes the conditions of load connected to Port 4 in different cases.

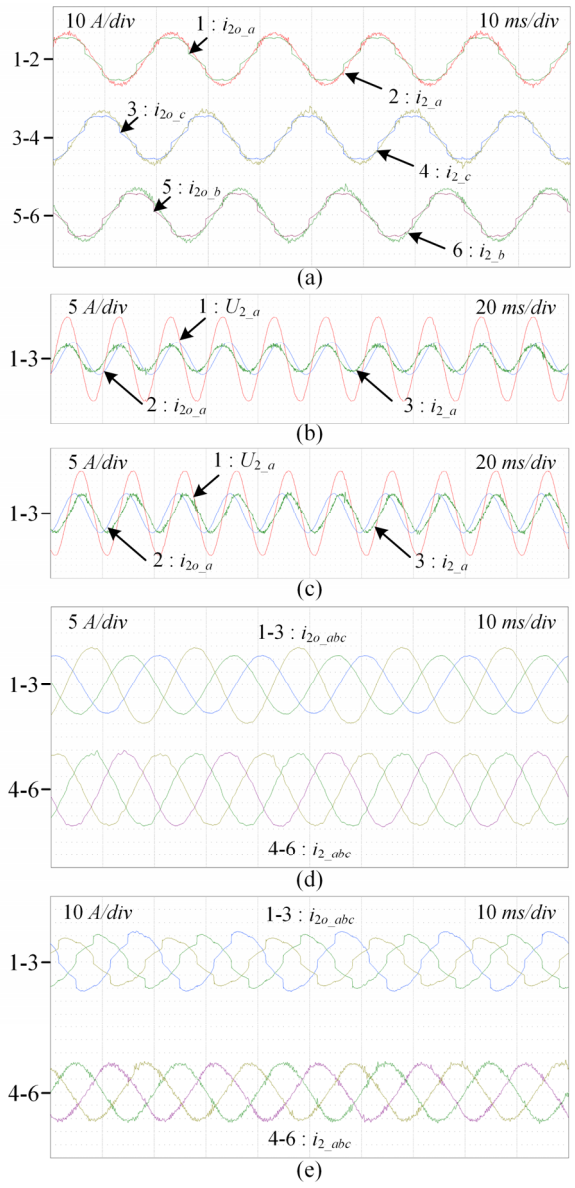

Fig. 10. *The experiment waveforms in Case C. (a) C-1, (b) C-2, (c) C-3, (d) C-4, (e) C-5.*

Table 4 The load condition in Case C.

Case	Load condition
C-1	Nonlinear loads (composed of a series connection of a diode bridge, a 79 Ω resistance).
C-2	A three-phase symmetric RC series load (each phase: 16 Ω and 250 μF).
C-3	A three-phase symmetric RL series load (each phase: 16 Ω and 75 mH).
C-4	A three-phase asymmetric R load (phase a: 32 Ω, phase b: 16 Ω, phase c: 32 Ω).
C-5	A parallel association of nonlinear loads (composed of a series connection of a diode bridge, a 79 Ω resistance), and a three-phase asymmetric RC series load (phase a: 16 Ω and 250 μF, phase b: 32 Ω and 250 μF, phase c: 16 Ω and 250 μF).

Table 5 and Table 6 show the calculated results of ER-MLFT in different cases. As shown in Table 5, THD of I_{2i_abc} and I_{2o_abc} is 12.39% and 3.21%, which verifies the effectiveness of the harmonic compensation function. Fig. 10 (b) and Fig. 10 (c) show the waveforms under different loads, and the results demonstrate that ER-MLFT has the function of reactive power compensation. In the case of C-4, Port 4 is connected to a three-phase asymmetric load and the neutral point of the load is suspended. The results indicate the effectiveness of the asymmetry compensation function. Fig. 10 (e) shows the experiment waveforms under complex load conditions. As shown in Table 6 and Fig. 10 (e), THD of I_{2o_abc} is 5.87%, and the third-harmonic content of I_{2o_abc} is 4.73 % of fundamental content due to asymmetry compensation. The results validate the effectiveness of reactive harmonic compensation, power compensation, and asymmetry compensation.

Table 5 The experimental results of Case C-1 to Case C-4.

PARAMETER	I_{2i_abc}	I_{2o_abc}
THD in case C-1/%	12.39	3.21
Power factor in case C-2	0.7511	0.9808
Power factor in case C-3	0.7246	0.9853
Three-phase current in case C-4/A	7.9, 10.4, 8.0	9.7, 9.6, 9.8

Table 6 The experimental results of Case C-5.

PARAMETER	I_{2i_abc}	I_{2o_abc}
THD/%	10.02	5.87
Three-phase current/A	15.7, 12.6, 13.5	14.7, 15.1, 14.7
Power factor	0.8971	0.9973
Third-harmonic content/%	0.25	4.73

6. Conclusion

A novel energy router based on the multi-winding line frequency transformer and power electronic devices is proposed in this paper. The proposed energy router can take advantage of the high reliability of the multi-winding line frequency transformer and the high controllability of power electronic devices. The hierarchical control strategy is employed, including the upper and lower level controls. The simulation and experimental results have been carried out to verify the effectiveness of the proposed energy router. As the characteristics of simple structure and flexible control, the proposed energy router is very suitable for the AC-DC hybrid grid with multiple voltage levels, and can also meet the high requirements of the smart grid.

7. References

[1] R. H. Lasseter, "Smart distribution: Coupled microgrids," *Proc. IEEE*, vol. 99, no. 6, pp. 1074-1082, June 2011.

[2] P. Li et al., "A lyapunov optimization-based energy management strategy for energy hub with energy router", *IEEE Trans. Smart Grid*, vol. 11, no. 6, pp. 4860-4870, 2020.

[3] A. Q. Huang et al., "The future renewable electric energy delivery and management (FREEDM) system: The energy Internet," *Proc. IEEE*, vol. 99, no. 1, pp. 133–148, Jan. 2011.

[4] D. Wang et al., "A 10-kV/400-V 500-kVA electronic power transformer," *IEEE Trans. Ind. Electron.*, vol. 63, no. 11, pp. 6653-6663, Nov. 2016.

[5] X. Gao et al., "Concurrent voltage control and dispatch of active distribution networks by means of smart transformer and storage", *IEEE Trans. Ind. Electron*., vol. 65, no. 8, pp. 6657-6666, Aug. 2018.
[6] W. Sheng et al., "Research of power distribution and application grid structure and equipment for future energy Internet," *Proc. CSEE*, vol. 35, no. 15, pp. 3760-3769, Aug. 2015.
[7] S. Hambridge, A. Q. Huang, and R. Yu, "Solid state transformer (SST) as an energy router: Economic dispatch based energy routing strategy," in *IEEE ECCE*, Montreal, QC, Canada, 2015, pp. 2355-2360.
[8] M. A. Hannan et al., "A review of Internet of energy based building energy management systems: Issues and recommendations," *IEEE Access*, vol. 6, pp. 38997-39014, Jul. 2018.
[9] Z. Zhao, G. Feng, L. Yuan, and C. Zhang, "The development and key technologies of electric energy router," *Proc. CSEE*, Vol. 37, no. 13, pp. 3823-3834, Jul. 2017.
[10] M. Gao et al., "Probabilistic model checking and scheduling implementation of an energy router system in energy Internet for green cities," *IEEE Trans. Ind. Inf.*, vol. 14, no. 4, pp. 1501-1510, Apr. 2018.
[11] S. M. S. Hussain et al., "Optimal Energy Routing in Microgrids With IEC 61850 Based Energy Routers," in *IEEE Trans. Ind. Electron.*, vol. 67, no. 6, pp. 5161-5169, June. 2020.
[12] B. Liu et al., "An AC–DC hybrid multi-port energy router with coordinated control and energy management strategies," *IEEE Access*, vol. 7, pp. 109069-109082, Aug. 2019.
[13] B. Liu, J. Chen, Y. Zhu, Y. Liu and Y. Shi, "Distributed control strategy of a microgrid community with an energy router", *IET Gener. Transmiss. Distrib.*, vol. 12, no. 17, pp. 4009-4015, Sep. 2018.
[14] B. Liu et al., "Design and implementation of multiport energy routers toward future energy Internet," *IEEE Tran. Ind. Appl.*, vol. 57, no. 3, pp. 1945-1957, May-Jun. 2021.
[15] S. Zheng et al., "SiC MOSFET based modular universal power electronics regulator," in *6th IEEE WiPDA*, Atlanta, GA, USA, 2018, pp. 32-39.
[16] J. E. Huber and J. W. Kolar, "Applicability of solid-state transformers in today's and future distribution grids," *IEEE Trans. Smart Grid*, vol. 10, no. 1, pp. 317-326, Jan. 2019.
[17] J. Miao et al., "Steady-state power flow model of energy router embedded AC network and its application in optimizing power system operation," *IEEE Trans. Smart Grid*, vol. 9, no. 5, pp. 4828-4837, Sept. 2018.
[18] Q. Duan et al., "Multi-port DC electric energy router based on cascaded high frequency transformer," *Power System Technology*, vol. 43, no. 8, pp. 2934-2941, Aug. 2019.
[19] D. Liang et al., "Analysis of development trend for intelligent distribution transformer," *Automation of Electric Power System*, vol. 44, no. 7, pp. 1-13. Apr. 2020.
[20] J. S. Lai et al., "Multifunction hybrid intelligent universal transformer," Patent U.S. 6954366, Oct. 11, 2005.
[21] M. Y. Hajmaharsi et al., "Hybrid distribution transformer with AC&DC power capabilities," U.S. Patent 20100201338, Aug. 12, 2010.
[22] S. Bala et al., "Hybrid distribution transformer: Concept development and field demonstration," in *IEEE ECCE*, Raleigh, NC, USA, 2012, pp. 4061-4068.
[23] P. Szcześniak and J. Kaniewski, "Hybrid transformer with matrix converter," *IEEE Trans. Power Delivery*, vol. 31, no. 3, pp. 1388-1396, Jun. 2016.
[24] J. Burkard and J. Biela, "Evaluation of topologies and optimal design of a hybrid distribution transformer," in *17th EPE'15 ECCE-Europe*, Geneva, Switzerland, 2015, pp. 1-10.
[25] J. Zhu et al., "A Novel Suppression Method for Grounding Transformer Against Earth Current From Urban Rail Transit," in *IEEE Trans. Ind. Electron.*, vol. 68, no. 12, pp. 11651-11662, Dec. 2021.
[26] S. Lin, S. Qin, R. Wang, and W. Wang, "Research of islanding mechanism and anti-islanding protection for DFIG," *Electric power automation equipment*, vol. 36, no. 7, Jul. 2016.